Supporting Information

Brown et al. 10.1073/pnas.1711155115

SI Experimental Procedures

Animals for SVF and JQ1 Treatment. C57BL/6J wild-type (WT) mice (male, 14 d old; Jackson Laboratory) were fed standard chow and were handled according to the Harvard Medical School IACUC guidelines. Stromal vascular cells were isolated from s.c. adipose depot by standard digestion protocol (1). Briefly, s.c. adipose depot was dissected from surrounding tissue. Sample was digested in a collagenase/dispase dissociation buffer for 30 min while rocking at 37 °C. Following digestion, samples were strained and washed with PBS to remove adipocyte fraction. Remaining cell pellet was resuspended and plated on collagen-coated plates. Differentation was performed with hormonal mixture as below. For treatment, 2-wk-old pups were treated with JQ1 (50 mg/kg per day) or vehicle control (IP, 12 d). JQ1 was prepared as previously described (2). Adipose tissue was harvested for analysis.

Adipocyte Differentiation. L1 and C3H10T1/2 cells were cultured and differentiated as previously described (3). Briefly, 10T1/2 cells were grown to confluence in DMEM supplemented with 10% FBS followed by adipogenic induction with 20 nM insulin and 1 nM T3, 0.5 mM IBMX, 1 μM dexamethasone, 0.125 mM indomethacin, and JQ1 or vehicle (DMSO) as indicated. For 3T3L1 cells, T3 and indomethacin were not included. After 48 h, media was supplemented with insulin and T3 (10T1/2) or insulin only (L1) every other day. For oil red O staining, cells were fixed in 10% formalin for 10 min then stained with oil red O. NIH 3T3 cells were differentiated with standard mixture supplemented with 5 μM rosiglitazone.

Reverse Transcription and Gene Expression. Total RNA was extracted (RNeasy; Qiagen), DNase-treated (Qiagen), and reverse-transcribed to cDNA. Gene expression, normalized to 36B4, was analyzed by quantitative real-time RT-PCR (Sybr Green) in 96-well plates using a MyiQ cycler (Bio-Rad). Primer sequences are provided in Dataset S2.

Nanostring Data Analysis. RNA was extracted as above and mixed with Nanostring reagents and probes as per manufacturer's protocol. Sample counts were corrected for background based on the mean of five negative controls. Counts were then scaled first to spiked positive controls and then by the geometric mean of four housekeeping genes (36B4, TUBB, β-actin, and GAPDH). Gene data for which fewer than 25% of samples had counts above background were excluded from analysis. Samples and genes were then clustered by Euclidean distance to reveal similarities in expression levels. Color is globally normalized with blue indicating lowest expression and red indicating highest fold change relative to untreated cells.

CRISPR Interference and Lentivirus Production. Individual gRNAs complementary to DNA at BRD4 binding sites in the Pparg super-enhancer were designed using a web-based, open source program (crispor.tefor.net). Sequences are provided in Dataset S2. Guides were cloned into a lentiviral transfer vector expressing dCas9-KRAB (plasmid 71236; Addgene) using a standard protocol (https://www.addgene.org/crispr/zhang). Sanger sequencing confirmed guide insertion. Lentivirus was generated by transfecting 293FT cells (Thermo Fisher) with guide-containing transfer plasmid (20 μg), packaging vector psPAX2 (15 mg, 12260; Addgene) and pMD2.G (7.5 mg, 12259; Addgene) with FuGENE HD in culture medium without antibiotics. After 12 h, media was changed to D10 + 1% BSA (high glucose DMEM supplemented with pyruvate, glutamine, 10% FBS, 1% BSA, sterile filtered). After 24 h, supernatant was removed and saved, and fresh D10 was added for another 24 h. Supernatant was combined, centrifuged at 1,700 × *g* for 10 min at 4° to pellet cell debris. Virus was concentrated 200-fold using PEG-IT (SBI), and cells were infected with 50 μL of virus along with Transdux Max (SBI). After virus transduction (24 h), media was changed and selection started with puromycin (10 μg/mL) at 48 h after virus. Cells were selected for 3 d and then cultured in standard growth media for experiments.

Coimmunoprecipitation. Nr3c1 mouse cDNA (clone 40111802; Dharmacon) was used as a template for BP cloning using standard attB primers and removal of the stop codon. Entry clone was confirmed by Sanger sequencing. This Nr3ca Entry clone was then LR cloned into lentiviral gateway vector with a preexisting V5 tag at the C terminus (pLEX306, 41391; Addgene). For Cebpb, we used a plasmid cloned into a Gateway Entry vector (Clone 100064071; Dharmacon). However, we first had to remove a preexisting stop codon (QuiKChangeII; Agilent) and then we LR-cloned Cebpb into the V5 lentivirus vector with a V5 tag at the C terminus. Virus was generated as described above, and 3T3L1 cells were transduced and stably selected using puromycin (10 μg/mL) for 72 h. Cells were then differentiated for 24 h in the presence of adipocyte differentiation mixture as described above. Following differentiation, nuclear protein was harvested per manufacturer's protocol (Active Motif, Nuclear Co-IP) and lysate incubated with V5 antibody-coated magnetic beads (MBL) overnight at 4° C. Protein was eluted by boiling in sample buffer, and lysate was separated by SDS/PAGE. Western bloting was performed with anti-V5 (R960-25; Thermo Fisher) and ant-BRD4 (A301-985A; Bethyl) antibodies followed by goat anti-mouse and goat anti-rabbit secondary antibodies (LiCOR). Two-color detection on an Odyssey scanner was used to detect protein signal.

Chromatin Immunoprecipitation. *L1* and *10T1/2* cells were grown to confluence in 15-cm plates (1×10^7 cells), treated with JQ1 in growth medium. Cells were cross-linked with 1% formaldehyde (10 min) followed by quenching (125 mM glycine). Cells were washed in cold PBS and harvested by cell scraper in cold PBS with protease inhibitors (Roche). Cells were centrifuged at 1,650 × *g* for 5 min. Pellets were resuspended in cytosolic then nuclear lysis buffer, and DNA was sheared on ice using a waterbath sonicator (Bioruptor; Diagenode) for 15 min at high output (30 s on, 30 s off), as previously described (4). Antibodies for ChIP: BRD4 (A301-985A; Bethyl), RNA polymerase II (sc-899; Santa Cruz). For ChIP, 5 μg of antibody was used for each IP.

Illumina DNA Sequencing and Library Generation. Purified ChIP DNA was used to prepare Illumina multiplexed sequencing libraries. Libraries for Illumina sequencing were prepared following the Illumina TruSeq DNA Sample Preparation v2 kit protocol with the following exceptions. After end-repair and A-tailing, immunoprecipitated DNA (~10–50 ng) or whole-cell extract DNA (50 ng) was ligated to a 1:50 dilution of Illumina Adapter Oligo Mix assigning one of 24 unique indexes in the kit to each sample. Following ligation, libraries were amplified by 18 cycles of PCR using the HiFi NGS Library Amplification kit from KAPA Biosystems. Amplified libraries were then size-selected using a 2% gel cassette in the Pippin Prep system from Sage Science set to capture fragments between 200 and

400 bp. Libraries were quantified by qPCR using the KAPA Biosystems Illumina Library Quantification kit according to kit protocols. Libraries with distinct TruSeq indexes were multiplexed by mixing at equimolar ratios and running together in a lane on the Illumina HiSeq 2000 for 40 bases in single read mode.

ChIP-Seq Data Analysis.

Accessing data generated in this work. All ChIP-Seq data generated in this publication can be found online associated with GEO Publication Reference ID GSE109940 (https://www.ncbi.nlm.nih.gov/geo/). For MED1, H3K27ac, and H3K4me3 ChIP-Seq, previously published datasets were used (GEO accession nos. GSM 1370466 and GSE21365, respectively).

Gene sets and annotations. All analysis was performed using RefSeq (NCBI37/MM9) mouse gene annotations.

ChIP-seq data processing. All ChIP-Seq datasets were aligned using Bowtie (version 1.0.0) to build version NCB37/MM9 of the mouse genome (5). Alignments were performed using the following criteria: -n2, -e70, -m1, -k1, -best. These criteria preserved only reads that mapped uniquely to the genome with one or fewer mismatches.

Calculating read density. We calculated the normalized read density of a ChIP-Seq dataset in any region as in ref. 6. Briefly, ChIP-Seq reads aligning to the region were extended by 200 bp, and the density of reads per bp was calculated. The density of reads in each region was normalized to the total number of million mapped reads producing read density in units of reads per million mapped reads per bp (rpm/bp).

Identifying ChIP-seq–enriched regions. We used the MACS version 1.4.2 (Model based analysis of ChIP-Seq) (7) peak finding algorithm to identify regions of ChIP-Seq enrichment over background. A P value threshold of enrichment of 1e-9 was used for all datasets. The GEO accession number and background used for each dataset can be found in Dataset S1.

Mapping enhancers and super-enhancers. Enhancers and super-enhancers were mapped using the ROSE software package described in refs. 8 and 9 and available at (younglab.wi.mit.edu/super_enhancer_code.html). In L1s, BRD4 and H3K27ac ChIP-Seq-enriched regions in either undifferentiated (D0) or differentiated conditions (D2) were used to map enhancers and super-enhancers.

Determining genomic localization of BRD4-binding sites. The genomic localization of BRD4 ChIP-Seq enriched regions in L1s was determined using the CEAS software (10). Promoter regions were defined as ±5 kb from the transcription start site. Gene body regions were defined as all regions contained inside annotated RefSeq transcripts outside of the promoter region. Intergenic regions were defined as all other regions in the genome (Fig. S3*A*).

Identifying candidate TF-binding regions from H3K27ac valleys. Regions between peaks of H3K27ac have been shown to harbor TF-binding sites (11). To identify these regions, we first defined the valleys in each enhancer region as described in ref. 12. Ten base-pair bins were assigned a valley score, then adjacent bins were stitched and their sequence was extended 100 bp on either side to search for TF binding motifs, as previously described (2).

Creating heatmap representations of ChIP-seq occupancy. Heatmaps of ChIP-Seq occupancy for various factors were created as in ref. 6. Heatmaps were created for the H3K27ac and K3K4me3 binding-enriched regions generated from public datasets of L1 differentiation. Each row plots the ±5-kb region flanking the center of the H3K4me3- or H3K27ac-enriched region. Rows are ranked by peak occupancy of H3K4me3 or H3K27ac (Fig. S3*C*).

Quantifying changes in super-enhancers. To quantify changes in super-enhancers between two conditions, background subtracted ChIP-Seq signal was calculated at the set of all enhancer regions considered super in at least one condition. Gained/lost super-enhancers were determined as those with a greater than twofold change signal in either direction. In L1s, changes in super-enhancers were determined by comparing BRD4 signal between undifferentiated and differentiated cells (Fig. 3*C*).

TF motif analysis. For the 365 gained and 54 lost super-enhancers, discrete BRD4 peaks were considered for motif discovery. All motifs from TFs expressed in either D0 or D2 adipocytes were considered using a motif database combined from Transfac, Jaspar, and curated literature sources. Motifs were searched using FIMO with a significance cutoff of 1e-5, and motif densities between the D0 and D2 enhancers were compared with derive TF motif enrichment scores.

1. Kajimura S, et al. (2009) Initiation of myoblast to brown fat switch by a PRDM16-C/EBP-beta transcriptional complex. *Nature* 460:1154–1158.
2. Brown JD, et al. (2014) NF-κB directs dynamic super enhancer formation in inflammation and atherogenesis. *Mol Cell* 56:219–231.
3. Kiefer FW, et al. (2012) Retinaldehyde dehydrogenase 1 regulates a thermogenic program in white adipose tissue. *Nat Med* 18:918–925.
4. Rahl PB, et al. (2010) c-Myc regulates transcriptional pause release. *Cell* 141:432–445.
5. Langmead B, Trapnell C, Pop M, Salzberg SL (2009) Ultrafast and memory-efficient alignment of short DNA sequences to the human genome. *Genome Biol* 10:R25.
6. Lin CY, et al. (2012) Transcriptional amplification in tumor cells with elevated c-Myc. *Cell* 151:56–67.
7. Zhang Y, et al. (2008) Model-based analysis of ChIP-seq (MACS). *Genome Biol* 9:R137.
8. Whyte WA, et al. (2013) Master transcription factors and mediator establish super-enhancers at key cell identity genes. *Cell* 153:307–319.
9. Lovén J, et al. (2013) Selective inhibition of tumor oncogenes by disruption of super-enhancers. *Cell* 153:320–334.
10. Shin H, Liu T, Manrai AK, Liu XS (2009) CEAS: cis-regulatory element annotation system. *Bioinformatics* 25:2605–2606.
11. Gerstein MB, et al. (2012) Architecture of the human regulatory network derived from ENCODE data. *Nature* 489:91–100.
12. Ramsey SA, et al. (2010) Genome-wide histone acetylation data improve prediction of mammalian transcription factor binding sites. *Bioinformatics* 26:2071–2075.

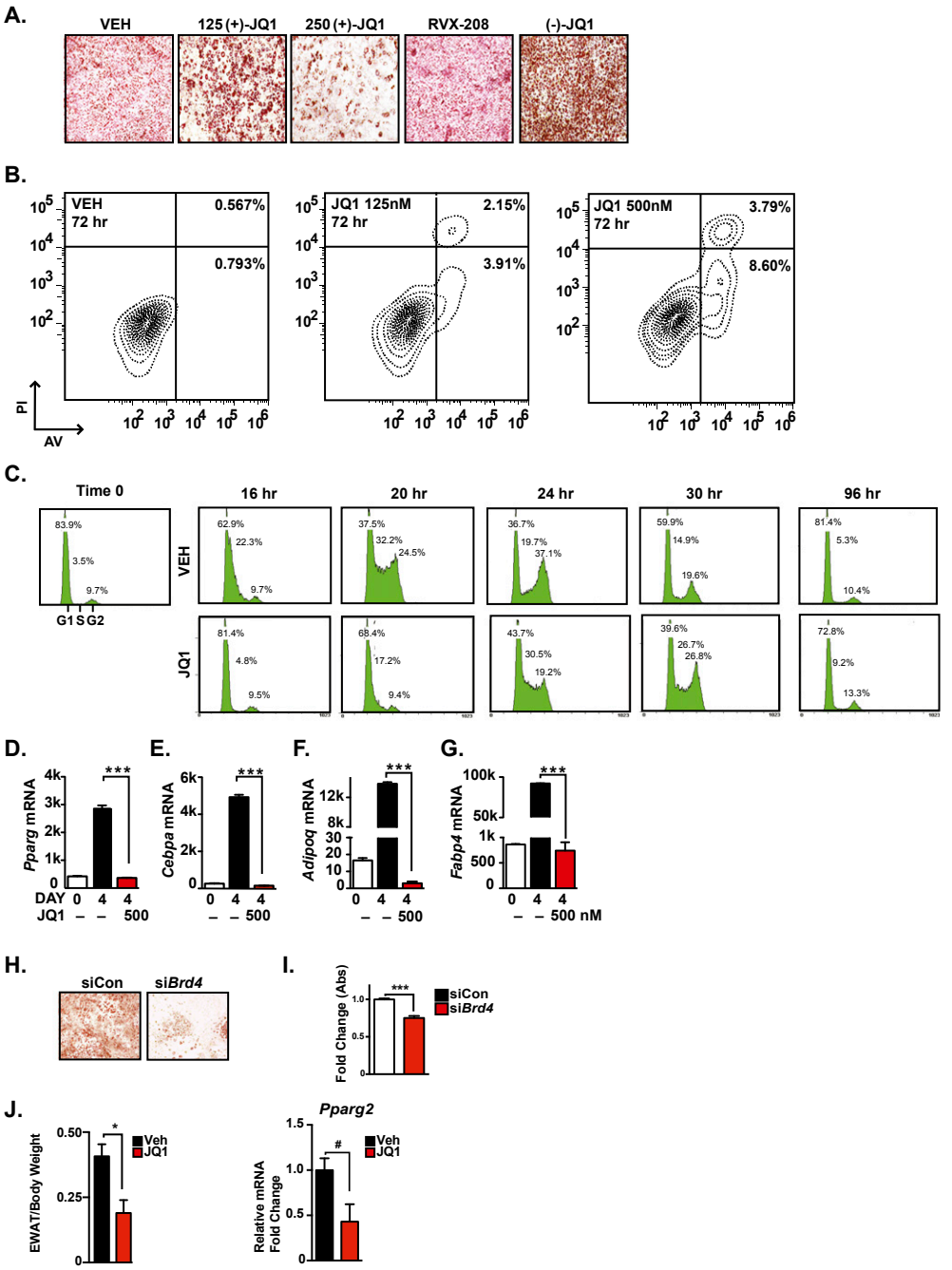

Fig. S1. Related to Fig. 1: BET bromodomain proteins control adipocyte differentiation. (*A*) Oil red O staining of L1 cells on day 8 of differentiation with or without structurally dissimilar BET bromodomain inhibitors. (-)-JQ1 (500 nM); RVX-208 (1 μM). (*B*) FACs plot of propidium iodide and annexin V-stained L1 cells differentiated in the presence of increasing concentrations of JQ1. Percentages indicate apoptosis (*Upper Right*, early apoptosis; *Lower Right*, late apoptosis). (*C*) FACs plot of cell cycle progression in L1 cells treated with vehicle or JQ1. Percentages indicate cells in G_1, S, or G_2 phase, respectively. (*D*–*G*) Bar plots of mRNA levels (nanostring) of *Pparg* (*D*), *Cebpa* (*E*), *Adipoq* (*F*), and *Fabp4* (*G*) from 3T3L1 cells treated as in Fig. 1*B*. (*H*) Oil red O staining of L1s differentiated after siRNA control or siRNA targeting Brd4. (*I*) Bar plot of fold change in absorbance from cells in *H* after extraction of oil red O. (*J*) Bar plots of epididymal white adipose tissue (EWAT) mass to body mass ratio (*Left*) and *Pparg2* mRNA expression (*Right*) in EWAT from mice treated with vehicle ($n = 4$) vs. JQ1 ($n = 3$). The statistical significance of the difference between vehicle (Veh) and JQ1 was determined using a two-tailed *t* test. (Magnification: 4×.) #$P = 0.05$, *$P < 0.05$, ***$P < 0.001$.

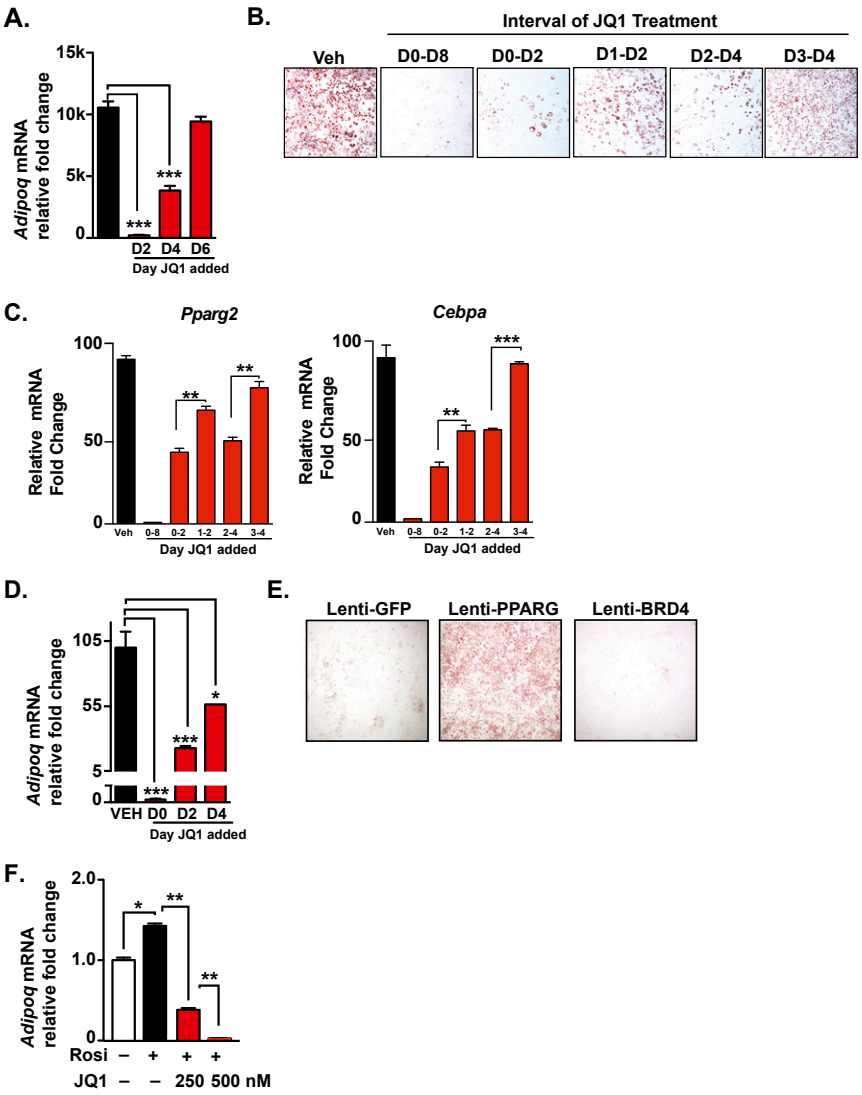

Fig. S2. Related to Fig. 2: BETs control expression of the master TFs *Pparg* and *Cebpa*. (*A*) Bar plot of relative expression levels of adiponectin (*Adipoq*) in L1 cells during differentiation ± JQ1 (500 nM). (*B*) Oil red O staining of L1s treated with JQ1 (500 nM) for different intervals of time followed by inhibitor washout. (*C*) Bar plots of *Pparg* and *Cebpa* mRNA expression in cells treated as in *B*. (*D*) Bar plot of relative expression levels of adiponectin (*Adipoq*) in 10T1/2 cells measured on day 6. (*E*) Oil red O staining of NIH 3T3 cells stably expressing GFP, PPARG, or BRD4 after differentiation (day 8). Cells were differentiated with standard mixture supplemented with rosiglitazone (5 μM) on D0–D2, followed by insulin and rosiglitazone after the first 48 h. (*F*) Bar plot of relative expression levels of adiponectin (*Adipoq*) in L1 cells treated with BET inhibition and rosiglitazone. Analysis was performed on day 8 for L1 and NIH cells and day 6 for 10T1/2 cells. The statistical significance of the difference between vehicle (Veh) or JQ1 was determined using a two-tailed *t* test. (Magnification: 4×.) $*P < 0.05$, $**P < 0.01$, $***P < 0.001$.

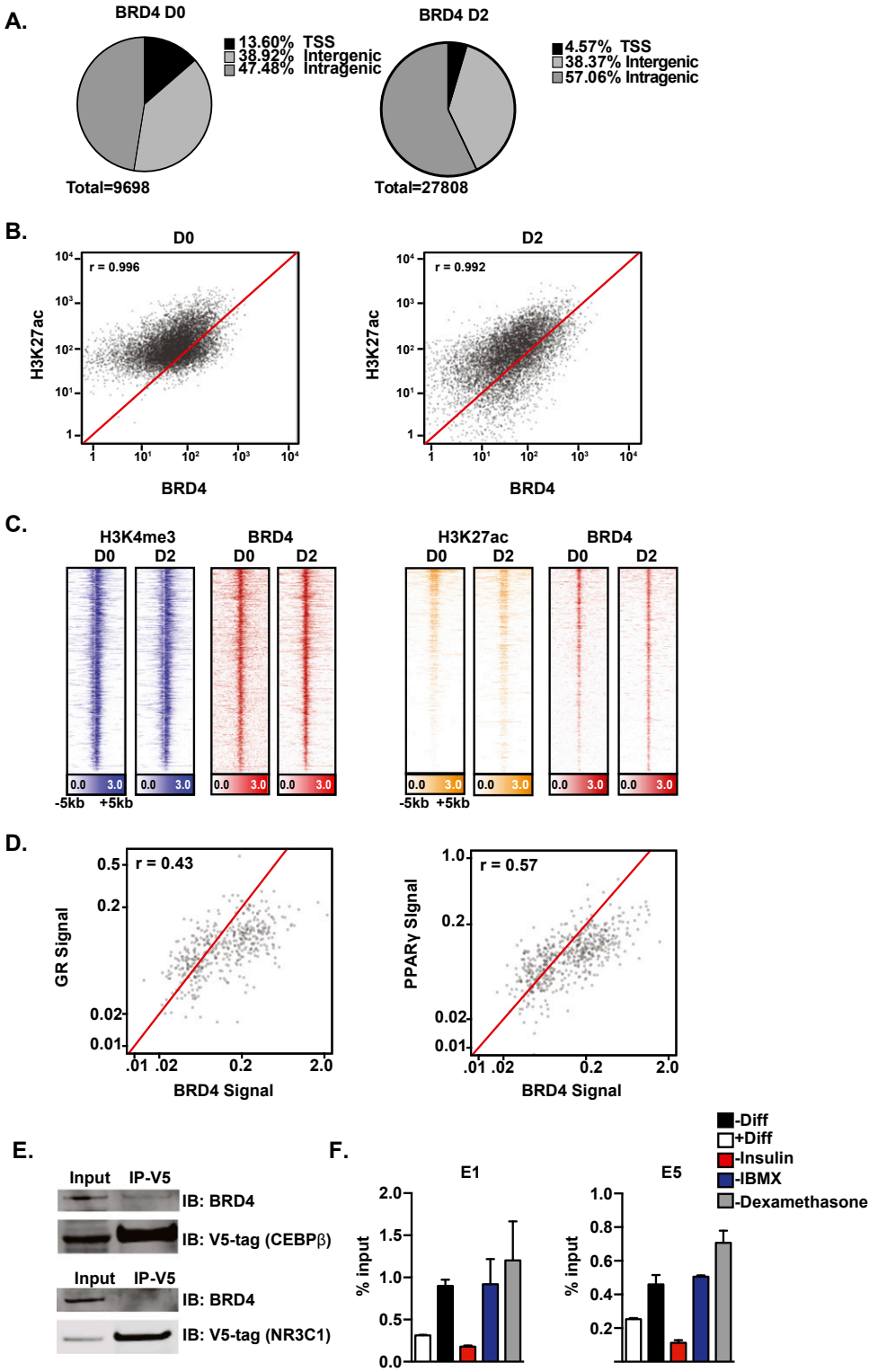

Fig. S3. Related to Fig. 3: Brd4 is dynamically redistributed to proadipogenic enhancers. (*A*) Pie chart of genomic distribution of BRD4 binding during L1 adipogenesis. (*B*) Scatter plot of BRD4 compared with H3K27ac at day 0 (D0) and day 2 (D2) of differentiation. (*C*) Heat maps of BRD4 localization during L1 adipogenesis at promoters ranked by K3K4me3 (*Left*) or enhancers H3K27ac (*Right*). (*D*) Scatter plot of BRD4 genomic localization compared with mapped binding sites for glucocorticoid receptor (GR) and PPARγ. (*E*) Western blot of BRD4 and V5 on L1 lysates after immunoprecipitation of V5-tagged CEBPβ (*Top*) or V5-tagged NR3C1 (*Bottom*). (*F*) Bar plots of BRD4 recruitment to enhancer sites within the *Pparg* locus measured by real-time ChIP-PCR (see Fig. 4 for the location of enhancer sites).

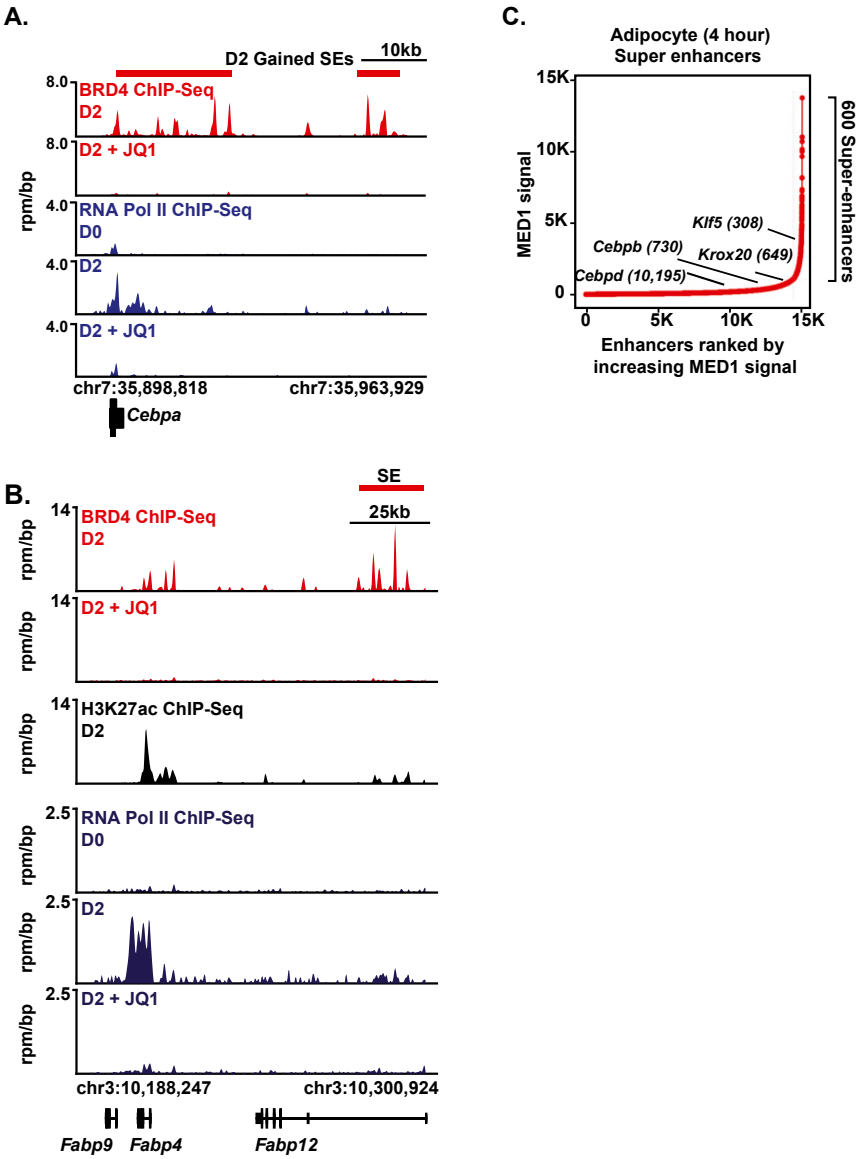

Fig. S4. Related to Fig. 5: Transcription of *Pparg* and *Cebpa* is BET bromodomain-dependent. (*A*) Gene track of ChIP-Seq signal for BRD4 (red) and RNA Pol II (dark blue) at the *Cebpa* locus showing change in BRD4 and RNA Pol II chromatin occupancy during L1 adipogenesis ± JQ1 (500 nM). (*B*) Gene track of ChIP-Seq signal for BRD4 (red), H3K27ac (black), and RNA Pol II (dark blue) at the *Fabp4* locus showing change in BRD4 and RNA Pol II chromatin occupancy during L1 adipogenesis ± JQ1 (500 nM). (*C*) Plot of enhancers in differentiating L1s (4 h after differentiation) ranked by increasing MED1 ChIP-Seq signal in units of reads per million (rpm).

Other Supporting Information Files

Dataset S1 (TXT)
Dataset S2 (XLXS)